Electrochemical Evaluation of a Corrosion Fatigue Failure Mechanism in a Duplex Stainless Steel

M.R. STOUDT and R.E. RICKER

Laboratory corrosion fatigue studies on smooth and precracked samples indicated that two duplex stainless steels would have similar service lives in a paper-processing environment; but, in service, one of these alloys has exhibited premature failures. Since corrosion fatigue experiments had proven unable to detect this failure mechanism, electrochemical measurements and slow strain rate tensile tests were used to evaluate four alloy composition-dependent failure mechanism hypotheses. No significant differences were found in the dissolution rates or hydrogen fugacities produced when mechanical processes expose bare surface, and slow strain rate tensile tests found no indication of a difference in cracking susceptibility for the same hydrogen fugacity. Electrochemical experiments found that pits nucleate in one phase of the duplex microstructure at lower potentials in the failure prone alloy, but do not propagate beyond the microscopic dimensions of this phase. These microstructurally limited "micropits" were found to nucleate fracture in slow strain rate tensile tests, and examination of a service failure confirmed the presence of microscopic pits at crack initiation sites. The premature failures are attributed to the lower pitting resistance of the failure prone alloy, and the failure of laboratory experiments to predict this behavior is attributed to the slow kinetics of pit nucleation in these experiments. A laboratory testing methodology is suggested that will ensure detection of similar susceptibilities in future corrosion fatigue testing programs.

I. INTRODUCTION

THE final stages of the paper-making process involve the separation of the processing solutions from the pulp slurry through the use of a series of cylindrical suction roll shells. These rolls are large hollow cast stainless steel cylinders about 1.0 m in diameter and up to 8.0-m long with wall thickness ranging from 50 to 100 mm. These tubes are perforated by a multitude of radial holes and moderate vacuums are employed to facilitate extraction of the processing solutions, as shown schematically in Figure 1.[1,2] A typical suction roll shell may experience more than 10^9 load cycles during a single year of operation, and the service lives of these rolls range between 5 and 8 years.[1] The combination of the rotational frequencies, cyclic stresses, and constant contact with highly aerated process solutions generates an aggressive service environment for these components. Hence, failure of these components has been a long-standing problem in this industry.[1,2,3]

The pulp and paper industry has conducted extensive laboratory-scale investigations into the corrosion fatigue behavior of alloys designed for this application using both tests on initially smooth samples (SN tests) and crack propagation experiments using precracked samples (*da*/*dN* tests). However, discrepancies still exist between laboratory measurement–based life predictions and actual performance in service.[2,4,5] One case of such a discrepancy concerns two duplex stainless steel alloys specifically developed for suction roll shells. These two alloys have similar microstructures and mechanical properties and differ primarily in that the failure resistant alloy has Cu added to the alloy.[6,7] Laboratory corrosion fatigue studies using both SN and *da*/*dN* tests over a range of frequencies and environments indicated that there should be little difference in the performance of these alloys in service; however, one alloy has consistently exhibited failures whereas no service-related failures have yet been reported for the other.[1,4–7] Some of the published SN and *da*/*dN* test results for these alloys are shown in Figure 2. While this figure shows that one alloy demonstrated slightly longer fatigue lives during SN testing and slower crack propagation rates, these differences are insufficient to explain why one fails in service while the other does not.

For this application, an alloy has been identified that performs satisfactorily in service, but it is not clear why laboratory experiments failed to correctly predict the performance of the other alloy. Without reliable laboratory experiments, uncertainties about actual performance in service will inhibit the development and application of new designs, alloys, or processes. The objective of this research was to determine why laboratory experiments failed to predict performance in this case so that this knowledge can be used to improve the reliability of similar studies in the future. The first step in accomplishing this objective is to identify the failure mechanism. Since the mechanical properties and microstructures of these two alloys are similar, it is assumed that the change in alloy composition altered the electrochemical behavior in such a way that a corrosion fatigue failure mechanism could operate in only one of the alloys during service, but not in either alloy during laboratory testing. Four hypotheses for this difference in the electrochemical (corrosion) behavior of these alloys and the resulting corrosion fatigue mechanism were developed and experiments were designed to evaluate each hypothesis.

M.R. STOUDT, Research Engineer, and R.E. RICKER, Metallurgist, are with the Metallurgy Division, Materials Science and Engineering Laboratory, National Institute of Standards and Technology, United States Department of Commerce, Gaithersburg, MD 20899-8553. Contact e-mail: richard.ricker@nist.gov

Manuscript submitted October 29, 2003.

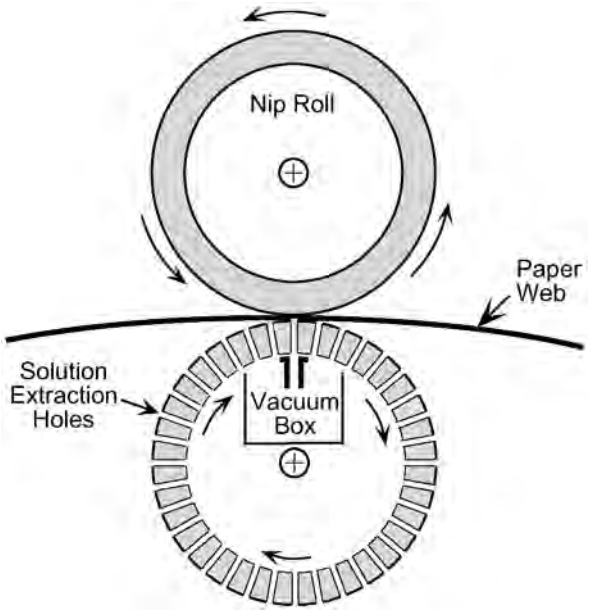

Fig. 1—Schematic illustration of the configuration of a suction press roll[1]

A. *Hypothesis I: Crack-Tip Dissolution Kinetics*

The first hypothesis was that changing composition altered the kinetics of alloy dissolution and repassivation. If the extent of dissolution per load cycle contributes to crack growth, then two alloys with different dissolution and repassivation kinetics may have similar crack propagation rates for one set of conditions and different rates for another set of conditions. While there is a range of conditions possible at a corrosion fatigue crack tip, this range is bounded by two fundamentally different extremes depending on whether anodic or cathodic reactions become rate limiting at the crack tip. Anodic reaction kinetics become rate limiting when cathodic reactions can remove the charge created by dissolution fast enough to prevent any significant changes in potential. Any factor that improves cathodic kinetics or increases the effective cathode to anode area ratio will drive the crack tip toward an anodic rate limiting condition. One of the most important of these factors is the effective resistance of the solution between the crack tip and cathodic sites on the external surface. This factor determines the area of cathode that can contribute to the removal of the charge created by the anodic reactions at the crack tip, and any factor that lowers this resistance will promote reaching anodic rate limiting conditions (short cracks, large crack openings, increased solution conductivity, *etc*.), which are influenced by testing conditions (*e.g*., loading frequency, mean load, crack geometry, *etc*.). This hypothesis was selected for evaluation because in service these factors may deviate significantly from those used for laboratory testing, and this could explain the discrepancy between laboratory and in-service behavior.

B. *Hypothesis II: Crack-Tip Hydrogen Fugacity*

The second hypothesis was that the difference in alloy composition altered the kinetics of crack-tip reactions such that a greater hydrogen fugacity could be produced at the crack tip of one alloy. If the effective conductivity of the solution in the crack becomes low (*e.g*., long tight cracks,

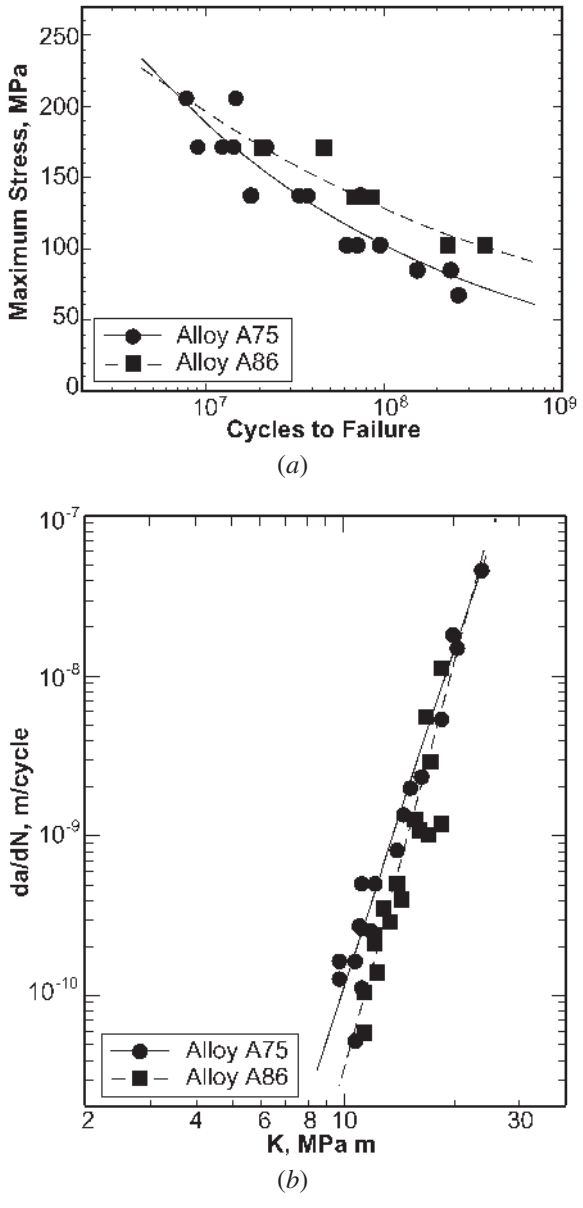

Fig. 2—Examples of published corrosion fatigue test results for (*a*) SN tests at 30 Hz and (*b*) *da/dN* tests at 25 Hz on alloys A75 and A86.[6,7]

corrosion product precipitation, solution drying, *etc*.), then the charge created by dissolution must also be removed by cathodic reactions at the crack tip. Unlike anodic reactions, the initial concentration of cathodic reactants on the freshly exposed bare surface at the crack tip is essentially zero and mass transport becomes rate limiting. When this occurs, the excess charge generated by anodic dissolution lowers the potential of the crack tip until the net rate of anodic and cathodic processes becomes equivalent and the potential stops decreasing. Then, the passive film starts reforming, which slows the rate of charge creation resulting in the potential returning to the initial value. The minimum potential during these transients determines the maximum hydrogen fugacity that can be produced at the crack tip.[8] This hypothesis was selected for evaluation for two reasons: (1) laboratory testing programs frequently do not consider cathodic rate limiting conditions, and (2) it was shown by Chatterjee *et al*.[9]

that adding a noble element to an alloy that promotes hydrogen evolution will suppress embrittlement.

C. *Hypothesis III: Susceptibility to Hydrogen-Induced Cracking*

The third hypothesis examined was that the change in alloy chemistry altered the hydrogen fugacity required to cause cracking. Even if the alloys experience the same hydrogen fugacities under cathodic rate-limited conditions, only one alloy might fail if it were embrittled at this fugacity while the other was not. A change in alloy chemistry could produce a difference in susceptibility by influencing segregation to grain boundaries and interphase interfaces that alter the cohesive strength of these interfaces and the influence of hydrogen on the strength of these interfaces. Transgranular cracking mechanisms could also be influenced by changes in alloy chemistry. This hypothesis was selected for evaluation because laboratory testing conditions might not produce hydrogen fugacities as great as those encountered in service, and alloying is well known to alter the susceptibility of alloys to hydrogen embrittlement.[10,11,12]

D. *Hypothesis IV: Susceptibility to Anodic-Induced Cracking*

The fourth hypothesis examined was that the change in alloy chemistry altered the resistance of the alloys to an anodically induced fracture mechanism. An anodically induced fracture mechanism is one where a feature or phase created by anodic reactions is responsible for crack nucleation or acceleration of crack propagation. In this case, either the geometry of the features or the properties of the phases created by corrosion are responsible for cracking, not the quantity of atoms dissolved from the crack tip. Stress corrosion cracking of pure Cu has been attributed to the nature and properties of the anodic surface films that form,[13,14] and there is evidence in the literature that anodic conditions can induce brittle cracking even in the absence of detectable amounts of anodic dissolution.[15–18] Since an anodic-induced fracture mechanism could occur under environmental conditions not evaluated during laboratory testing, this hypothesis was also selected for evaluation.

II. EXPERIMENTAL

A. *Materials and Environment*

Samples of the two alloys, designated A75 and A86, were obtained and the compositions of these alloys are shown in Table I. The percent change in concentration for each element in these two alloys is also included in this table, and it can be seen that the primary difference in these alloys is the increase in the Cu content of the failure resistant alloy (A86) compared to the failure prone alloy (A75). However, in addition to having a greater Cu content, this alloy has an increased concentration of Si (+54 pct) and reduced S (−73 pct), C (−18 pct), and N (−17 pct) contents. The duplex microstructures of these alloys are shown in Figure 3. The differences between the microstructures shown in this figure are well within the range of variations observed for large castings made from these alloys.

Table I. Nominal Alloy Compositions

Element	A75 Mass Pct	A75 Mol Pct	A86 Mass Pct	A86 Mol Pct	Pct Chg A75-A86
C	0.017	0.077	0.014	0.064	−17.6
Mn	0.760	0.755	0.800	0.795	+5.3
Si	0.500	0.972	0.770	1.496	+54.0
Cr	25.390	26.652	26.070	27.357	+2.7
Ni	6.700	6.229	6.800	6.320	+1.5
Mo	0.030	0.017	0.030	0.017	0.0
N	0.066	0.257	0.055	0.214	−16.7
P	0.032	0.056	0.032	0.056	0.0
S	0.011	0.019	0.003	0.005	−72.7
Cu	0.180	0.155	2.080	1.786	+1.055
Fe	66.314	64.811	63.346	61.890	−4.5

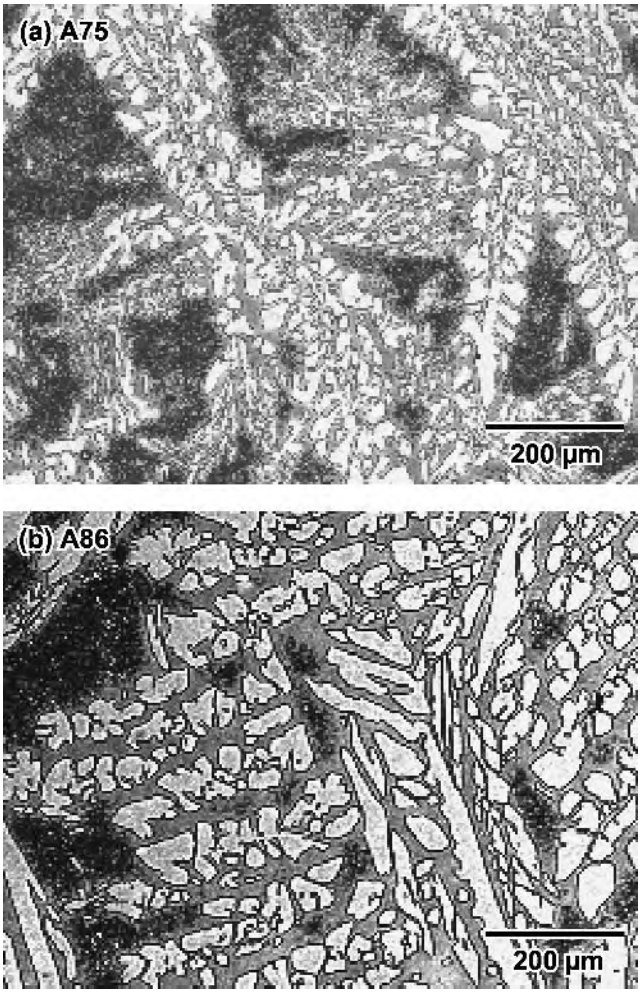

Fig. 3—Optical micrographs showing the duplex structure of the alloys: (*a*) alloy A75 and (*b*) alloy A86 (Viella's etch: gray—ferrite, white—austenite).

A solution and temperature representative of the processing conditions where the corrosion fatigue failures occurred was selected for these tests. The composition of this solution, known as simulated deinked white water (DWW), is identified in Table II and all experiments were conducted at 50 °C. The electrochemical experiments included variations in this solution composition, but all results presented are for

Table II. Chemistry of the Simulated White Water Solution

Anion	Concentration
$(SO_4)^{-2}$	500 mg/L
$(Cl)^{-}$	200 mg/L
$(S_2O_3)^{-2}$	50 mg/L
(Cation: Na^{+})	Solution pH: 3.9 ± 0.1

this composition.[19] While this solution is considered representative of the papermaking environment, it should be kept in mind that actual service environments include biological species that secrete species and produce surface scales that this solution does not include.[1,2,4–7]

B. *Repassivation Current Measurements*

To evaluate hypothesis I, the anodic reaction rate-limited repassivation behavior of the alloys was quantified by measuring the current required to repassivate mechanically generated bare surface at a constant potential. The bare surface was generated by *in-situ* scratching of lacquer-coated samples with a sapphire scribe in the simulated DWW environment at 50 °C. The lacquer coating was used to eliminate currents to regions of the sample outside the scratch. A commercial potentiostat was used to maintain anodic reaction rate-limited conditions by providing the current as required to keep the potential of the sample constant, and the current was recorded with a digital oscilloscope. The response of the measurement instrumentation was optimized in the same manner as previous studies of Al alloys and intermetallic compounds.[20,21] Optimization in this relatively low conductivity solution required a bare Pt wire as the reference electrode to reduce impedance. The Pt wire reference electrode was encased in glass or coated with lacquer, except for two sections on either side region, which were to be scratched (≈2-mm long, 3 mm apart, and 1 mm from the surface). The potential of the Pt reference electrode was measured against a saturated calomel electrode (SCE) before and after scratching, and the alloys were scratched at the same potential (−0.30 V *vs* SCE).

The electrodes for these experiments were constructed by mounting 1-mm-thick samples of the alloys on edge in epoxy metallurgical mounts and polishing them to a 1.0-μm diamond surface finish.[22] Electrical contact was made through the back of the samples with copper wires isolated from the environment by polytetrafluoroethylene sleeves. The exposed surfaces of the polished samples were coated with lacquer and the samples were scratched through this thin lacquer coating to eliminate stray currents. The sapphire scribe was driven across the sample at a velocity of ≈1 m/s by a dropping weight.[20,21] The scratch velocity was determined for each individual scratch from the length of the scratch and the points in the time record that indicated the start and end of the scratch. The length and width of the scratches were measured in a microscope ($\pm 0.5 \times 10^{-6}$ m resolution) and the area estimated using these measurements and measurements of the shape of the sapphire scribe. No corrections were made for surface roughness. This experimental method was specifically designed to produce a bare surface at a nearly constant rate during the scratching process to enable analysis by fitting the resulting transients to a convolution integral, as suggested by Alder and Walters.[20,23–25]

C. *Repassivation Potential Measurements*

To evaluate hypothesis II, the hydrogen fugacity produced by film rupture under cathodic reaction rate-limited conditions was quantified by measuring the potential transients that result when bare surface is generated under galvanostatic conditions with zero current flow. As discussed in Section II-B, the bare surface was generated through *in-situ* scratching of samples in the simulated DWW environment at 50 °C, but for these experiments, the charge generated by dissolution is not allowed to leave the region of the scratch. Current flow is minimized by measuring potential with a high-impedance voltmeter ($>10^{12}$ Ω) and scratching the sample through a lacquer coating. The potential was measured with a SCE using a Luggin capillary, and a digital oscilloscope recorded the potential transients. It should be kept in mind that the scale of the scratches generated in these physical models of film rupture events is significantly larger than that of the microstructural features. Thus, the scratches are microstructural averages, while the scale of actual film rupture events may be small enough to be contained within a single phase or boundary.

D. *Slow Strain Rate Tensile Tests*

To evaluate hypothesis III, slow strain rate (SSR) tensile tests were conducted at cathodic potentials at a strain rate of 1×10^{-6}/s in simulated DWW at 50 °C.[19,26–28] Hypothesis IV was evaluated by conducting SSR tests at anodic potentials identified by the electrochemical measurements. For the SSR experiments, cylindrical samples with gage sections 25-mm long and 3.15 mm in diameter were machined from centrifugally cast suction roll shells of each alloy with the tensile axis parallel to the long axis of the casting. The gage sections were polished to a 1.0-μm diamond surface finish, and the surfaces outside the gage section were coated with lacquer. A 250-mL double walled glass environmental chamber connected to a closed-loop temperature controller that circulated water between the cell walls was used to hold the environment and keep the solution at 50 °C ± 1.0 °C during these experiments. The intrinsic (inert environment) mechanical properties were determined by conducting tests at the same strain rate and temperature in dry nitrogen gas. After failure, the samples were removed from the testing chamber, rinsed in flowing water, dried, and stored in vacuum until they were examined in a scanning electron microscope.

E. *Free-Corrosion Potential Time Series*

The range and variability of the oxidizing conditions that the alloys would experience in service were assessed by measuring the free-corrosion potentials (FCP) of the alloys in the DWW environment and variations in this environment at 10-second intervals for 24 hours. The term "free corrosion" is used to indicate that the sample is corroding in the environment under open circuit conditions, where it is free from the influence of any reactions or currents other than those produced on its own surface. The electrodes for

these experiments were fabricated by mounting 6.35-mm cylindrical samples of the alloys in epoxy metallurgical mounts with electrical contact through the back of the mount in the same manner discussed in Section II-B. The samples were polished to a 1.0-μm diamond surface finish using standard metallurgical practice.[22] The experiments were conducted in a double-walled glass electrochemical cell containing $\approx$125 mL of solution connected to a closed-loop temperature controller, which circulated water between the cell walls to keep the solution at 50 °C $\pm$ 1.0 °C. The potentials of the samples were measured against an SCE with a Luggin capillary and a computer-controlled, high-impedance ($>10^{12}$ Ω) digital voltmeter.

F. *Potentiodynamic Polarization Current Measurements*

Potentiodynamic polarization experiments were used to compare the electrochemical behavior of the alloys. Samples for these experiments were prepared in the same manner as samples for the FCP measurements, and the experiments were conducted in the same chamber. A commercial high-gain closed-loop amplifier (potentiostat) was used with an SCE and a carbon counter electrode to measure and provide the current required for each potential as the potential was scanned at 20, 5, or 1 mV/s. The potential ranges of these scans were varied to enable better resolution of differences in the alloys. For deaerated conditions, the cell was sealed and the solution was purged of oxygen by bubbling nitrogen through it for at least 20 minutes prior to insertion of the sample after which the nitrogen flow was diverted to continuously purge the space above the solution. For the aerated condition, the cell was left open to laboratory air. For clarity of presentation, only the currents measured while the potential was moving in the positive direction are presented.

III. RESULTS

A. *Repassivation Current Measurements*

These experiments were designed to determine if the change in alloy composition alters the crack-tip dissolution and repassivation kinetics under anodic reaction rate-limited conditions. Figure 4 shows a representative repassivation current transient for each alloy. Examination of these curves shows that the measured current increases in a linear manner during scratching, reaching a maximum when the scribe exits the sample after which the current decays toward a steady-state value. While the current increase during scratching is almost linear, it always curved below the tangent defined by the initial values before scratching was complete. The consistent and reproducible nature of this deviation indicates that repassivation initiated on surfaces made bare at initiation of the scratch before scratching was complete. While this observation does not prevent estimation of the bare surface current density from the initial tangent slope, it indicates that an analysis of the current decay that assumes that the entire surface was made bare instantaneously would result in errors. As a result, the current transients were analyzed by fitting the results to an equation derived by convolution of a bare surface generation function and a repassivation function, as suggested previously.[20,23–25] A repassivation function of the type used by Adler and Waters[24] to represent repassivation of a 304 stainless steel provided an excellent fit to these results. This equation is

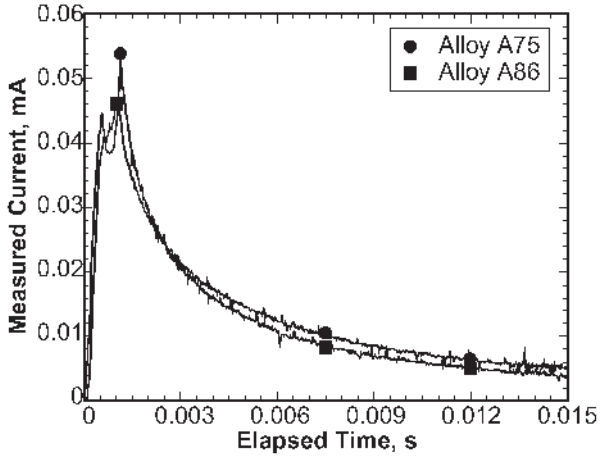

Fig. 4—Scratch repassivation current transients for the alloys in aerated deinked white water at 50 °C and −0.30 V *vs* SCE.

$$i(t) = i_B\left[\frac{t}{t_B}\right]^n \qquad [1]$$

for $t \geq t_B$ and

$$i(t) = i_B \qquad [2]$$

for $t \leq t_B$, where i_B is the bare surface current density, n is the repassivation exponent, and t_B is the average time an increment of surface area remains bare after being exposed by scratching. The convolution of this equation with the linear bare surface generation function results in dividing the current response into four time periods with respect to the scratch duration time (t_S): (1) $t \leq t_B$, (2) $t_B \leq t \leq t_S$, (3) $t_S \leq t \leq (t_S + t_B)$, and (4) $t \geq (t_S + t_B)$. The bare surface current density, i_B in Eq. [1], was determined by fitting the current and area measurements to the solution for the convolution integral for the rise transient of the first time period:

$$I(t) = i_B A\left[\frac{t}{t_S}\right] \qquad [3]$$

where $I(t)$ is the measured current and t_S is the duration time of the scratch determined from the transient. The bare surface current density determined from this fit (i^*_B) was then used to estimate n and t_B by fitting the current measurements for times greater than $(t_S + t_B)$ to the solution of the convolution integral for the fourth time period:

$$I(t) = \frac{i^*A}{t_S}\left[\frac{t^{n+1} - (t - t_S)^{n+1}}{t_B^n(n+1)}\right] \qquad [4]$$

The curve fitting was accomplished using commercial curve fitting software that uses an iterative Levenberg–Marquardt algorithm for nonlinear least-squares curve fitting.[29] This process was repeated on three different repassivation current transients for each alloy to assess the experimental and fitting scatter. This examination found no significant difference between the alloys for t_B and n, while i_B was less for

the failure prone alloy (A75) than the Cu-rich alloy (A86), as shown in Table III.

B. *Repassivation Potential Measurements*

These measurements were designed to emulate crack-tip behavior under cathodic reaction rate-limited conditions where the active potential transient could result in hydrogen evolution and absorption into the crack-tip plastic zone. For these experiments, the potential transient that accompanies the creation of bare surface by scratching under conditions where all reduction reactions must also occur on the freshly generated bare surface is measured with a reference electrode, since this quantity is related through equilibrium thermodynamics to the fugacity of hydrogen generated by reduction on this surface.[8] Figure 5 shows representative potential transients for the alloys in the simulated DWW environment at 50 °C, and a hydrogen equilibrium fugacity ordinate is included to show the significance of these potential transients. These curves typically consist of three regions. First, an initial potential drop of several hundred millivolts occurs when the first increment of bare surface comes into contact with the solution. This entire drop is not shown in the figure so that the details of the other regions can be seen. Second, during the remainder of the approximately 1 ms required for the scribe to traverse the sample, the potential will oscillate about some mean value that typically decreased slightly during this stage (usually <50 mV). Once the scratch is complete and the bare surface is no longer being generated, the third region of behavior is observed where the potential increases toward the range of steady-state free corrosion potentials. The minimum potentials (E_{min}) and initial rates of potential, which increase following completion of the scratch (dE/dt_{in}) are given in Table IV. A statistical analysis (Student's *t*-test) of these results confirmed that the observed differences in the alloys are not significant compared to the experimental scatter.[30] That is, these measurements failed to detect any evidence that this change in alloy composition alters the fugacity of hydrogen that will be produced at crack tips under cathodic rate-limited conditions.

Table III. Parameters Determined by Curve Fitting for Potentiostatic Scratch-Repassivation Current Transients

Scratch Number	Alloy	i_B (A/m^2)	t_B (mS)	n
1	A75	714	0.338	−0.455
2	A75	1081	0.516	−0.329
3	A75	894	0.170	−0.341
4	A86	1514	0.241	−0.526
5	A86	1215	0.355	−0.450
6	A86	1628	0.290	−0.375
Average	A75	896	0.341	−0.421
Standard deviation	A75	184	0.173	0.084
Average	A86	1452	0.295	−0.375
Standard deviation	A86	213	0.057	0.070
Average	A75 + A86	1174	0.318	−0.467
Standard deviation	A75 + A86	353	0.118	0.081

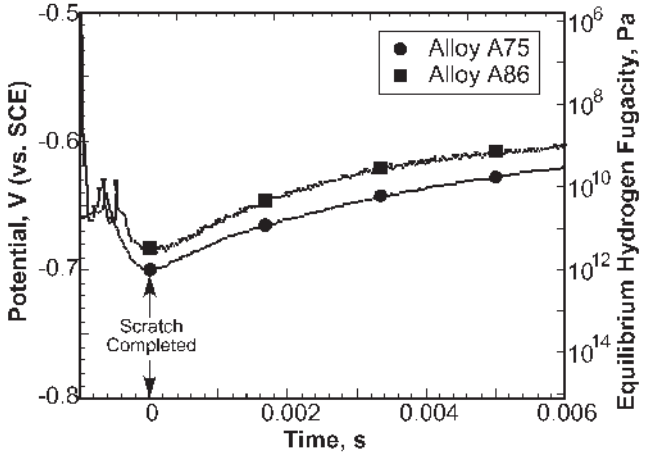

Fig. 5—Scratch repassivation potential transients for the alloys in aerated, deinked white water at 50 °C with the equivalent equilibrium hydrogen fugacities shown on the right axis.

C. *SSR Tests at Cathodic Potentials*

Since the repassivation potential measurements indicated that there is no difference in the activity of hydrogen that can be produced at crack tips in these alloys, SSR tensile tests were conducted to evaluate the influence of hydrogen fugacity on the mechanical properties of these alloys. To facilitate graphical interpretation of these results, a ductility ratio was calculated for each of these experiments, and these values are plotted against the fixed electrode potential of the sample during the test in Figure 6. Examination of these data shows cathodic polarization to potentials below the free-corrosion potential but above the hydrogen evolution potential results in ductilities that approach those of inert environments

Table IV. Scratch-Repassivation Potential Transient Data

	Alloy A75		Alloy A86	
Scratch Number	E_{min} (V_{SCE})	dE/dt (V_{SCE}/s)	E_{min} (V_{SCE})	dE/dt (V_{SCE}/s)
1	−0.554	19.8	−0.415	12.9
2	−0.837	180.0	−0.417	6.3
3	−0.701	52.0	−0.780	52.2
4	−0.771	58.6	−0.812	55.6
5	−0.639	97.2	−0.666	194.6
Average	−0.700	81.5	−0.618	64.3
Standard deviation	0.111	61.5	0.192	76.2

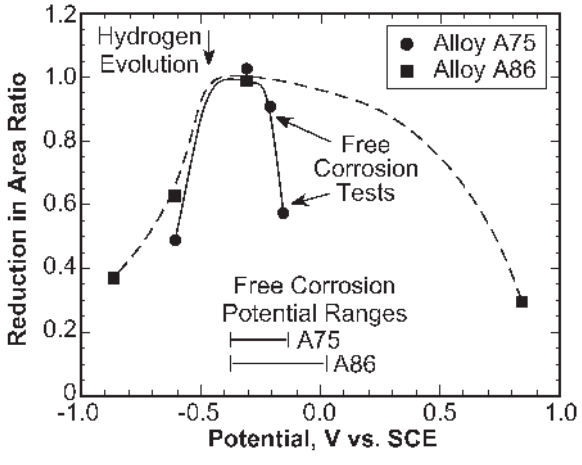

Fig. 6—Reduction in area ductility ratio as a function of potential in free corrosion and potentiostatically controlled slow strain rate tensile tests.

or air. However, cathodic polarization below the hydrogen evolution potential, which is ≈ -0.475 V *vs* SCE for this solution and temperature, results in reduced ductility for both alloys. Reduced ductilities were observed at the free corrosion potential for the failure prone alloy (A75) and at an anodic potential for the Cu-rich alloy (A86).

D. *FCP Time Series*

Time-series measurements of the free corrosion potentials of the alloys in aerated DWW at 50 °C were used to evaluate the range of oxidizing or reducing conditions the alloys would experience in service. The free corrosion potentials of the alloys in this environment varied over a range of values, but after examining the time record of a number of 24-hour tests, it was determined that the free corrosion potentials did not vary about a stationary mean in a purely random manner. Some consistent trends and differences in the behavior of the alloys could be identified, as shown in Figure 7. First, on insertion into the solution, the free corrosion potentials of both alloys tended to increase with time, eventually reaching a steady-state value after several hours of exposure. This observation is consistent with the assumption that the air-formed passive film is thinner or otherwise less protective than the steady-state film that forms in DWW at 50 °C. The main difference in the behavior of the alloys was that while the potential of Cu-rich alloy (A86) would move steadily toward its steady-state value and reach it in a few hours, the potential of the failure prone alloy (A75) would oscillate erratically over a range of potentials for 10 to 14 hours before reaching steady state. In addition, the steady-state potential of this alloy was about 100 mV below that of the Cu-rich alloy (A86).

E. *Potentiodynamic Polarization Current Measurements*

Figure 8 shows representative potentiodynamic polarization curves for the alloys in aerated and deaerated simulated DWW at 50 °C. Initially, these experiments revealed little difference in the behavior of these alloys over the range of potentials between hydrogen evolution and oxygen evolution, but occasionally, the failure prone alloy (A75) would exhibit a different behavior, as shown by the curve marked with open circles in Figure 8(a). This behavior was difficult to reproduce, but examination of these samples in the optical microscope revealed that the austenite phase of this alloy contained microscopic pits. This result, in conjunction with the observation of erratic potential swings during the FCP measurements, indicated that metastable pitting occurred in the austenite phase of this alloy during free corrosion in this environment. To enable better determination of the potential where pitting starts, significantly larger samples were tested in deaerated DWW solution at 50 °C. The results of these experiments, shown in Figure 8(b), indicated that pitting occurred in this alloy at much lower potentials than the failure-resistant alloy, and the potential where this behavior starts is close to the steady-state free corrosion potential for this alloy. Examination in an optical microscope after potentiostatic holds in this potential range confirmed that pitting was the source of this increased current. Similar experiments on the Cu-rich, failure-resistant, alloy (A86) confirmed that this alloy was not pitting at the same potentials. Pitting did occur in this alloy (A86) at potentials well above the FCP range for this alloy and environment.

F. *Fractography*

Examination of the fracture surfaces of samples tested in nitrogen gas at 50 °C revealed that both alloys exhibited

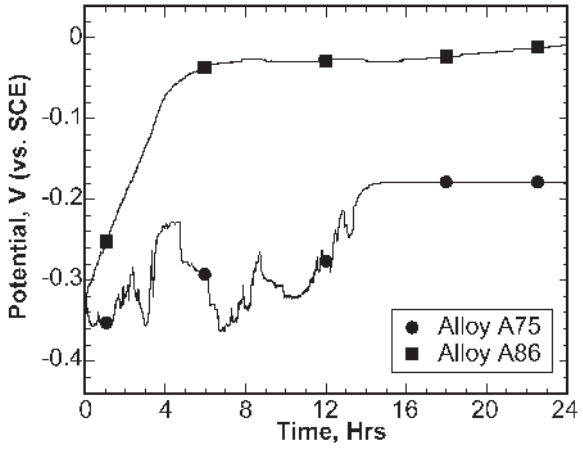

Fig. 7—Potential time record of alloys A75 and A86 while freely corroding in aerate-simulated deinked white water at 50 °C for 24 h.

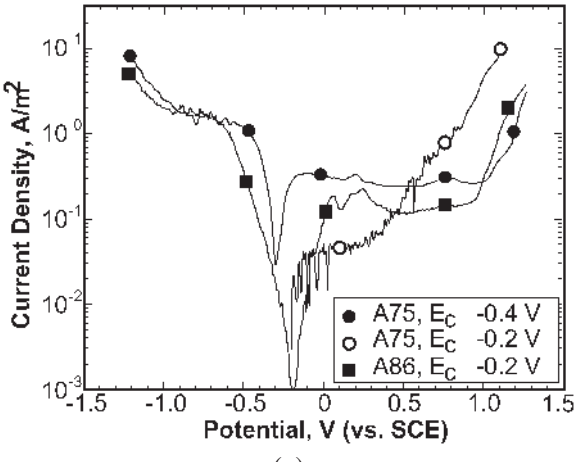

(*a*)

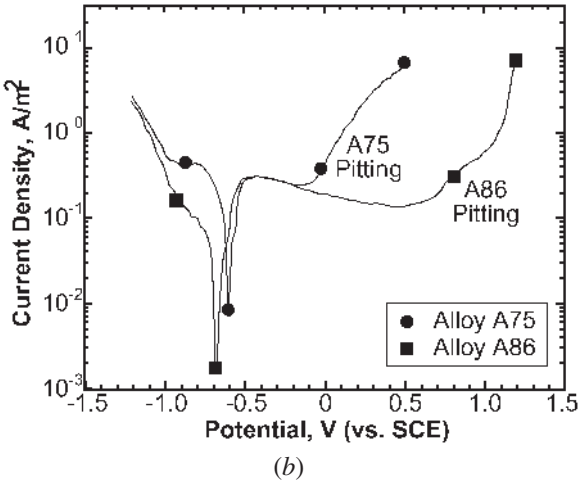

(*b*)

Fig. 8—Potentiodynamic polarization curves in simulated deinked white water at 1 mV/s: (*a*) aerated solution with electrode areas 32 mm^2 and (*b*) deaerated solutions with electrode areas 285 mm^2.

approximately equal areas of ductile, microvoid coalescence (MVC) and a transgranular fracture mode that is cleavage-like in appearance, as shown in Figure 9. This transgranular "cleavagelike" (TCL) fracture mode is probably the result of alternating shear or some other mechanism,[17,18] but analysis of this mechanism is beyond the scope of the present work. These morphologies were bound by the interphase interface with TCL restricted to the ferrite phase and MVC observed in the austenite phase. No unambiguous exceptions could be found for this phase-specific segregation of fracture morphologies in the nitrogen environment. Examination of the fracture surface of a sample of the failure prone alloy tested under free corrosion conditions revealed selective pitting of the austenite phase, as illustrated in Figure 10(a). To determine if similar attack would occur in A86 during anodic polarization, a sample of this alloy was tested at a potential above the pitting potential of this alloy and nearly identical behavior was observed, as shown in Figure 10(b). Failure analyses had not reported this behavior, but the service environment produces heavy scales on the exposed surfaces that could prevent observation of these small pits. As a result, a section of an A75 service failure was obtained, carefully cleaned, sectioned, and examined to determine if small pits similar to those observed in this study were present at the site of fatigue crack initiation. Figure 11 is a representative micrograph showing a fatigue crack that initiated at the base of a very small pit.

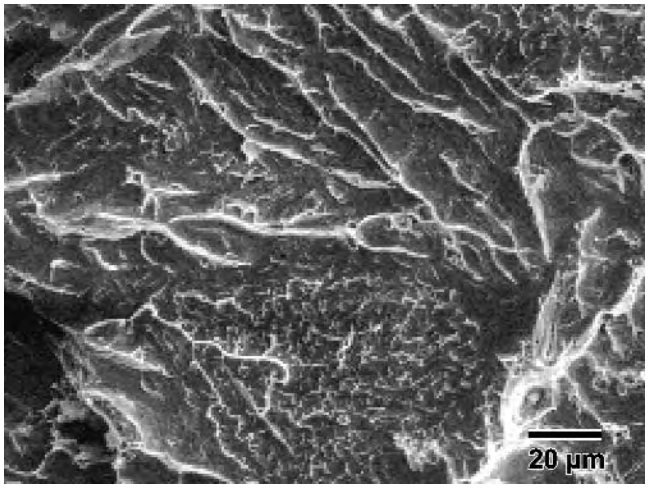

Fig. 9—Scanning electron micrograph of the fracture surface on alloy A75 in nitrogen gas at 50 °C.

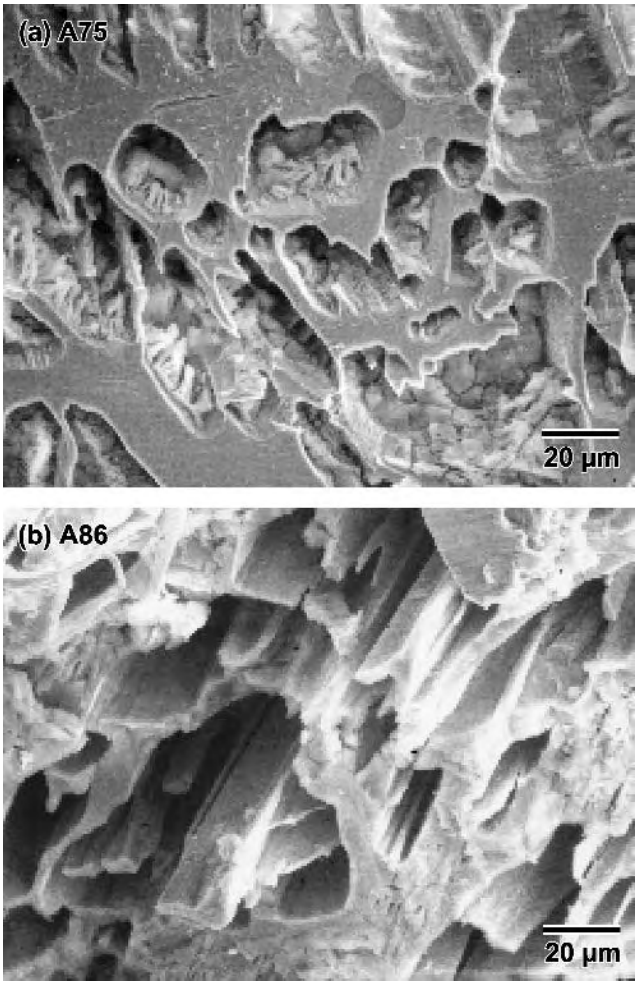

Fig. 10—Scanning electron micrographs of the pitting attack observed on the polished surfaces of the alloys in simulated deinked white water at 50 °C: (*a*) alloy A75 freely corroding and (*b*) alloy A86 anodically polarized to +0.85 V *vs* SCE.

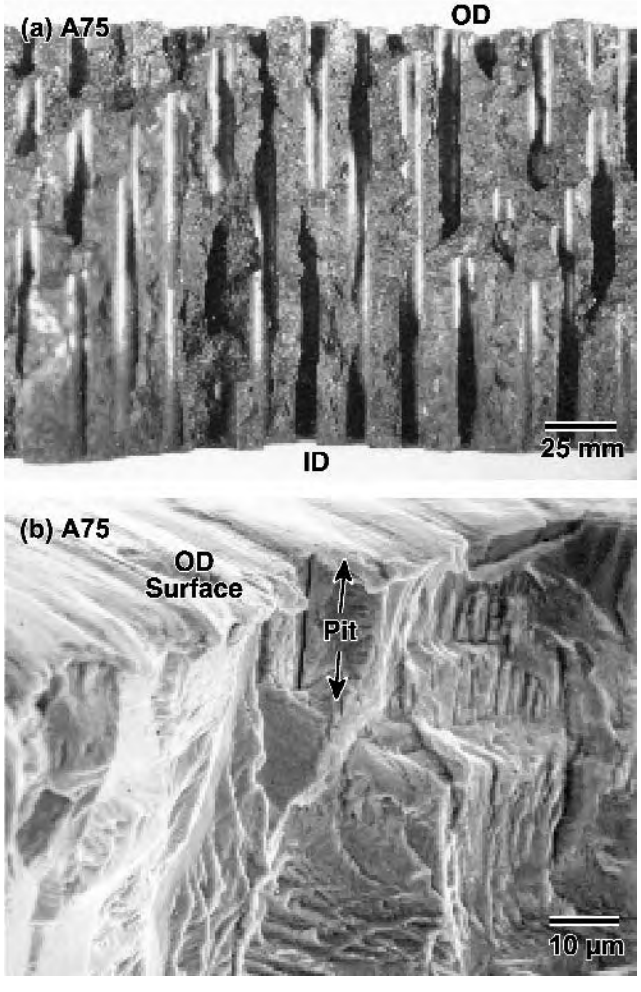

Fig. 11—(*a*) Macrograph and (*b*) scanning electron micrograph of a service failure showing a corrosion pit at the initiation site of a fatigue crack.

IV. DISCUSSION

A. *Failure Mechanism*

Four mechanistic hypotheses were evaluated: (I) crack-tip dissolution kinetics, (II) crack-tip hydrogen fugacity, (III) susceptibility to hydrogen-induced cracking, and (IV) susceptibility to anodic induced cracking. Electrochemical measurements and cracking susceptibility measurements were used for these evaluations because (1) previous investigations using laboratory corrosion fatigue tests had not detected a significant difference in the behavior of these alloys, (2) it was clear that a difference in corrosion behavior was the cause, (3) electrochemical measurements would yield more fundamental information on differences in corrosion behavior and, therefore, the origin of these failures, and (4) electrochemical measurements could be used to guide future laboratory corrosion fatigue studies and prevent missing similar failure mechanisms in other systems.

In the case of the first two hypotheses, electrochemical experiments were designed specifically for the evaluation of the fundamental electrochemical properties that could determine performance under different rate-limiting extremes. While both scratch repassivation current and potential transients have been used by previous investigators to understand passivity for many years,[31] previous work was concerned primarily with producing data for modeling stress corrosion cracking or corrosion fatigue crack propagation rates or for comparing the pitting behavior of alloys.[20,21,32–35] This is the first time that these two types of experiments have been used together to compare the anodic and cathode rate-limiting conditions for fatigue cracks in two alloys. Even though no significant difference was revealed by these tests, ruling out any contribution of a difference in repassivation rates was a significant result that dramatically reduces ambiguity in the conclusions of this study.

Hypotheses III and IV were evaluated by assessing cracking susceptibility with slow strain rate tensile tests under controlled electrochemical conditions. For hypothesis III (susceptibility to hydrogen cracking), identification of the electrochemical conditions for these tests was a simple matter of calculating the potential where the hydrogen fugacity was sufficient to cause hydrogen evolution and absorption into the alloys. No significant difference in susceptibility was found. For hypothesis IV (susceptibility to anodic induced cracking), the electrochemical behavior of the alloys was surveyed to identify conditions where the behavior of the alloys may be different. A potential range was identified where higher anodic currents were observed occasionally in the failure prone alloy. This behavior was examined in greater detail.

Anodically induced cracking (hypothesis IV) is the only mechanism consistent with all of the observations of this study. The results show that anodic conditions can result in the nucleation and propagation of pits in either alloy. However, these pits nucleate at much lower potentials in the failure prone alloy. Since these pits propagate in only one phase, their growth is limited to the microscopic dimensions of this phase in the fine microstructures of these alloys. This makes these micropits difficult to detect, but also creates pits with sharp cracklike features. Clearly, these sharp features will initiate fatigue cracking when exposed to cyclic loading. Initially, it was assumed that confirmation of the mechanism in this study would require fatigue testing under conditions identified by the electrochemical experiments. This proved unnecessary when the microscopic examination of a service failure revealed microscopic pits at crack initiation sites identical to those found in the electrochemical experiments.

B. *Detection of Pitting*

The difficulty in identifying pitting as the source of this behavior was due to the combined influence of the microstructure of these alloys and the relatively low conductivity of this environment. Although crystallographic facets and other microstructural features are sometimes observed during pitting, pits in most alloys and environments grow with smooth interior surfaces and a hemispherical shape.[36] The rapid current increases normally observed when pits nucleate are the combined result of the rapidly increasing bare surface area and the large overpotential (excess free energy) for dissolution of the bare surface in the pit.[37,38] Confining the pits to one phase of this fine microstructure prevents the bare surface area from increasing rapidly after nucleation and forces the pits to grow with high aspect ratios (depth/width). This dramatically increases the magnitude of the potential drop between the mouth and the tip of the pit. Since potential drop in the pit determines how deep a pit can propagate before it repassivates, the high aspect ratios imposed by the microstructure plus the low conductivity of this environment combine to keep these pits very small. Furthermore, the pits have sharp microstructural features that, while not looking like classical pitting, concentrate stress and initiate crack propagation.[39,40]

In addition to the size and morphology of the pits, the heavy deposits typically found on service failures make detection difficult. In the electrochemical experiments, the small size and morphology of these pits inhibits detection by obstructing nucleation and limiting propagation. Pits did not always nucleate during potentiodynamic polarization experiments, and after nucleation, the current increased at a much lower rate than that typical of pitting in stainless steels (Figure 8). The difficulty of nucleating stable pits is also illustrated by the extended period required for free corrosion potential of the failure prone alloy (A75) to reach steady state (Figure 7). In these experiments, the erratic shifts in potential are almost certainly due to the nucleation and repassivation of metastable pits, and the steady-state potential reached after 12 hours is essentially the pitting potential determined in Figure 8. To produce potentiodynamic polarization curves with reproducible pitting potentials, as shown in Figure 8(b), experiments were conducted on larger samples (to expose more area and a wider range of microstructure feature sizes) and in a thoroughly deaerated solution (to prevent the nucleation of pits before the scans started).

C. *Performance in Service*

The experimental results indicate that the difference in the pitting potentials of these alloys is the critical factor that determines the behavior in service. The rationale for this conclusion is the observation that the pitting potentials (Figure 8) and the free corrosion potentials (Figure 7) for the two alloys in aerated solutions indicate there is a very high probability that the failure prone alloy (A75) will pit in

service, while there is a very low probability that the failure-resistant alloy (A86) will pit in service. Since it is well know that pits with sharp features can initiate fatigue crack propagation,[39,40] the difference in the pitting behavior of these alloys is the only factor capable of explaining the difference in the performance of these alloys in service. Therefore, it is concluded that this difference in pitting behavior is responsible for the difference in performance in service.

Considering that the Cu content is the most significant difference in the composition of these two alloys, it would appear that the difference in the pitting resistance of these alloys is due to the influence of this element. Pitting could also be due to chromium depletion or segregation of a passivity-inhibiting element, such as sulfur, to the ferrite-austenite interface and the changes in the Si, C, and S contents of the alloys may also contribute.[41] While Cu is usually found to exert a beneficial influence on the pitting resistance of stainless steels, this is not universally observed and the literature is inconclusive on the nature of this effect.[42,43,44] These seemingly contradictory results in the literature could also be an indication that Cu influences the behavior of some other element. Since Cu is more soluble in the austenite phase,[44] it will segregate to this phase and the ferrite-austenite interface will have a Cu concentration gradient that may influence the segregation of other elements and the phases present at this interface. Evaluation of the origin of the beneficial influence of Cu will require experiments with carefully modified and thoroughly characterized alloy chemistries beyond the scope of the present work. Hence, it remains unclear at this time whether Cu additions enhance passivity, prevent chromium depletion, or inhibit the segregation or action of a passivity-inhibiting element in these alloys.

Increasing the rate of repassivation is frequently invoked as means of improving the pitting resistance of an alloy or to explain a difference in the pitting resistance of two alloys. Clearly, the results of these experiments create doubt on this mechanism for the beneficial influence of Cu. Even though these experiments essentially average the behavior of the phases in the alloys, a delay in the repassivation of any region should produce a resolvable difference in the transients. While the scatter in the measurements casts some doubt on this conclusion, the results indicate that other mechanisms should be considered to explain the beneficial influence of Cu. Additional experiments on carefully produced single-phase microstructures on similar alloys or with other alloying elements known to improve pitting resistance are necessary to resolve this uncertainty.

D. *Performance in Laboratory Fatigue Tests*

As pointed out in Section I, the real motivation for this work was to determine why laboratory experiments failed to predict that failures would occur in service. Crack propagation tests are not sensitive to external surface conditions and pitting will not occur at the crack tip because the solution in this region will be relatively deaerated. In contrast, SN tests are highly sensitive to the surface condition of the sample, making them an excellent means to evaluate the influence of surface treatments on fatigue crack initiation.[45,46] Therefore, if pitting occurred prior to fatigue crack initiation during SN testing of any sample of A75, then it would have certainly lowered the observed fatigue life. As a result, it must be assumed that pitting did not occur during these tests before fatigue cracks initiated by their normal initiation mechanism.

The experimental results of this study support this explanation. For example, in Figure 7, the free corrosion potential of A75 did not exceed the potential required for stable pit growth until after 14 hours of exposure. This is 10^4 to 10^6 cycles at normal SN fatigue testing frequencies. During this 14-hour incubation period, the potential exhibited erratic behavior possibly indicating the formation of metastable pit nuclei, but either this behavior did not influence fatigue crack initiation or cyclic loading suppressed this behavior. Cyclic loading could help suppress pitting by periodically exposing bare surface at persistent slip bands (PSBs) and crack nuclei that will react and consume oxygen lowering the potential of the sample. Basically, each PSB will undergo a transient similar to those shown in Figure 5, but since the PSB area is a small fraction of the sample area, the effect of a single event on the overall potential of the sample will be small; however, the sum of these events over time could be significant depending on sample size, solution volume, loading frequency, and other testing conditions.

E. *Recommended Practice for Corrosion Fatigue Testing*

Future testing programs can ensure that this or similar failure mechanisms have not been overlooked by conducting fatigue tests over the entire range of corrosion potentials expected in service. Currently, most testing programs emulate the service environment and test samples as they corrode in this environment without any external influence (*i.e.*, free corrosion). Since potential is proportional to the thermodynamic forces driving corrosion, this approach allows the single most important parameter determining behavior to vary randomly during the tests and assumes that these random variations can represent the entire range of conditions that may occur during service. As Figure 7 illustrates, this assumption may not always be valid; and in this case, it appears to be responsible for the failure to accurately predict performance in service. Potential measurements could be used and tests repeated until the entire range of conditions expected in service has been evaluated, but it may be less wasteful to identify the range of solution compositions and potentials expected in service and test over that entire range (plus a safety factor) using a potentiostat to control potential. A thorough characterization of the corrosion fatigue behavior would still require both SN and crack propagation tests. This approach would quantify performance over the entire range of expected corrosion conditions and driving forces, producing more reliable conclusions about the ability of an alloy to withstand the rigors of a particular application.

V. CONCLUSIONS

The objective of this research was to determine why laboratory experiments failed to accurately predict performance of alloy A75 for this application. Four hypotheses were developed for a corrosion fatigue failure mechanism that could operate in service and not be observed during laboratory experiments. These hypotheses were systematically evaluated and it was found that a defect generated by corrosion

in service, but not during laboratory testing, was the most likely cause of the failure of laboratory tests to accurately predict performance. A service failure was examined, which confirmed the presence of these defects at the failure initiation sites.

The defects identified as responsible for initiating fatigue crack propagation were small pits caused by the selective dissolution of the austenite phase in the susceptible alloy. The fine microstructure of these alloys and the low conductivity of this environment kept these pits from growing beyond microscopic dimensions and the scales formed in service inhibited their detection. These "micropits" did not stimulate failure during laboratory fatigue tests because they are the result of passive film breakdown (pitting corrosion) and require nucleation. Apparently, the testing conditions used for laboratory fatigue tests were not sufficiently oxidizing or the tests were too brief for these micropits to nucleate. These results indicate that conducting fatigue tests (SN and *da*/*dN*) over the entire range of environmental conditions expected in service, including corrosion potentials through the use of a potentiostat, will enable the detection of this and similar corrosion fatigue failure mechanisms for future applications.

ACKNOWLEDGMENTS

The authors express their appreciation to J. Rogers, A. Castillo, and G. Michel, Sandusky International, Inc., for supplying the materials used in this investigation and for their technical input and assistance throughout.

REFERENCES

1. R.A. Yeske: *Mater. Performance*, 1987, vol. 26, pp. 30-37.
2. C.E. Jaske and A.P. Castillo: *Mater. Performance*, 1987, vol. 26, pp. 37-43.
3. D.C. Reid and D.A. Wensley: *TAPPI J*., 1989, Mar., pp. 57-61.
4. R.M. Yeske, M.A. Revall, and C.M. Thompson: *TAPPI J*., 1994, vol. 77, pp. 210-17.
5. R.A. Yeske: *TAPPI J*., 1988, Mar., pp. 47-54.
6. A.P. Castillo, G.M. Michel, and J.C. Rogers, *TAPPI J*., 1989, vol. 72, pp. 193-97.
7. A.P. Castillo and G.M. Michel: *TAPPI J*., 1992, vol. 75, pp. 131-38.
8. J.O.M. Bockris and A.K.N. Reddy: *Modern Electrochemistry*, Plenum Press, New York, NY, 1970, vol. 2.
9. S.S. Chatterjee, B. Ateya, and H.W. Pickering: *Metall. Trans. A*, 1978, vol. 9A, pp. 389-95.
10. N.R. Moody, A.W. Thompson, R.E. Ricker, G.S. Was, and R.H. Jones: *Hydrogen Effects on Material Behavior and Corrosion Deformation Interactions*, TMS, Warrendale, PA, 2003.
11. M.F. Fernandes: Ph.D. Dissertation, University of Notre Dame, Notre Dame, IN, 1989.
12. A.W. Thompson: in *Envrionment-Sensitive Fracture of Engineering Materials*, Z.A. Foroulis, ed., TMS, Warrendale, PA, 1977, pp. 379-410.
13. T.B. Cassagne: Ph.D. Dissertation, The Johns Hopkins University, Baltimore, MD, 1988.
14. T.B. Cassagne, J. Kruger, and E.N. Pugh: in *Environmentally Assisted Cracking: Science and Engineering*, W.B. Lisagor, T.W. Crooker, and B.N. Leis, eds., ASTM STP 1049, ASTM, Philadelphia, PA, 1989, pp. 59-75.
15. U. Bertocci, F.I. Thomas, and E.N. Pugh: *Corrosion*, 1984, vol. 40, pp. 439-40.
16. K. Sieradzki and R.C. Newman: *Phil. Mag. A*, 1985, vol. 51, pp. 95-132.
17. R.H. Jones and R.E. Ricker: in *Metals Handbook*, 9th ed., J.R. Davis, ed., ASM INTERNATIONAL, Metals Park, OH, 1987, pp. 145-63.
18. R.H. Jones and R.E. Ricker: in *Stress-Corrosion Cracking: Materials Performance and Evaluation*, R.H. Jones, ed., ASM INTERNATIONAL, Materials Park, OH, 1992, pp. 1-40.
19. M.R. Stoudt: Report No. NISTIR 6309, NIST, Gaithersburg, MD, 1999.
20. M.R. Stoudt, A.K. Vasudevan, and R.E. Ricker: *New Methods for Corrosion Testing of Aluminum Alloys*; V.S. Agarwala and G.M. Ugiansky, eds., ASTM STP 1134, ASTM, Philadelphia, PA, 1992, pp. 196-213.
21. R.E. Ricker: *Mater. Sci. Eng*., 1995, vol. A198, pp. 231-38.
22. G.F. VanderVoort: *Metallography Principles and Practice*, McGraw-Hill, New york, NY, 1984, pp. 410-502.
23. M. Barbosa: *Corrosion* 1988, vol. 44, pp. 149-53.
24. T.A. Adler and R.P. Walters: *Corrosion*, 1993, vol. 49, pp. 399-408.
25. I.S. Sokolnikoff and R.M. Redheffer: *Mathematics of Physics and Modern Engineering*, McGraw-Hill, New York, NY, 1966.
26. M.R. Stoudt, J.L. Fink, J.F. Dante, and R.E. Ricker: *Fire Suppression System Performance of Alternative Agents*, NIST Special Publication 890, R.G. Gann, ed., NIST, Gaithersburg, MD, 1995, pp. 121-200.
27. M.R. Stoudt, J.L. Fink, and R.E. Ricker: *J. Mater. Eng. Performance*, 1996, vol. 5, pp. 507-15.
28. G. Santarini: *Corrosion*, 1989, vol. 45, pp. 369-81.
29. D.M. Bates and D.G. Watts: *Nonlinear Regression Analysis and Its Application*, John Wiley & Sons, Inc., New York, NY, 1988.
30. W. Mendenhall and T. Sincich: *Statistics for Engineering and the Sciences*, 3rd ed., Dellen Publishing Co., San Francisco, CA, 1992.
31. M. Faraday and C.T. Schönbein: *Phil. Mag*., 1836, vol. IX, pp. 53-65.
32. T. Hagyard and J.R. Williams: *Trans. Faraday Soc*., 1961, vol. 57, pp. 2288-94.
33. T. Hagyard and W.B. Earl: *J. Electrochem. Soc*., 1967, vol. 114, p. 694.
34. T. Hagyard and M.J. Prior: *Trans. Faraday Soc*., 1961, vol. 57, pp. 2295-98.
35. R.E. Ricker, U. Bertocci, J.L. Fink, and M.R. Stoudt: in *Environmental Effects on Advanced Materials*, R.H. Jones and R.E. Ricker, eds., TMS, Warrendale, PA, 1991, pp. 213-25.
36. T.P. Hoar: *Corr. Sci*., 1967, vol. 7, p. 341.
37. H.H. Uhlig: *Corrosion and Corrosion Control*, John Wiley & Sons, New York, NY, 1971.
38. C.A. Hampel: *The Encyclopedia of Electrochemistry*, Reinhold Publ., New York, NY, 1964.
39. J.H. Payer and R.W. Staehle: in *Corrosion Fatigue*, A.J. McEvily and R.W. Staehle, eds., NACE International, Houston, TX, 1972, pp. 211-69.
40. S. Suresh: *Fatigue of Materials*, Cambridge University Press, Cambridge, United Kingdom, 1991.
41. P. Marcus: *Corrosion Mechanisms in Theory and Practice*, P. Marcus and J. Oudar, eds., Marcel Dekker, New York, NY, 1995, pp. 239-64.
42. M. Stern: *J. Electrochem. Soc*., 1955, vol. 102, pp. 663-68.
43. A. Moskowitz, G.A. Saltzman, K.E. Pinnow, and L.S. Redmerski: *Effects of Residual Elements on the Properties of Stainless Steels*, R.B. Gunia, ed., ASTM STP 418, ASTM, Philadelphia, PA, 1967, pp. 3-22.
44. A.J. Sedriks: *Corrosion of Stainless Steels*, J. Wiley & Sons, Inc., New York, NY, 1979.
45. M.R. Stoudt, R.C. Cammarata, and R.E. Ricker: *Scripta Mater*., 2000, vol. 43, pp. 491-96.
46. M.R. Stoudt, R.E. Ricker, and R.C. Cammarata: *Int. J. Fatigue* 2001, vol. 23, pp. 215-23.